Journal of *Marine Science and Engineering*

MDPI

Article

Spreading Magnetic Anomalies Separation of the South China Sea Based on the Nested Elliptical Directional Filters

Mingming Wang [1,2,*], Song Chen [1] and Herong Gui [1]

[1] School of Resources and Civil Engineering, Suzhou University, Suzhou 234000, China
[2] School of Earth and Space Sciences, University of Science and Technology of China, Hefei 230026, China
* Correspondence: wmm@ahszu.edu.cn

Abstract: Spreading magnetic anomalies recorded the paleo-geomagnetic field variation that has great significance in the investigation of the extension process of ocean basins. Interpreting spreading magnetic anomalies under complex geological environments is challenging, especially for marginal sea basins. We proposed nested elliptical directional filters to separate the spreading magnetic anomalies of the South China Sea (SCS). The results show that the spreading magnetic anomalies separated by the nested elliptical directional filters depict the expansion process of the oceanic crust, and the interference magnetic anomalies are effectively suppressed. The separated spreading magnetic anomalies indicate that the expansion process of the SCS is affected by the interactions between the surrounding plates. The spreading magnetic anomalies of the SCS are warped, interrupted, and not strictly parallel. The pattern of the spreading magnetic anomalies reflects multiple ridge jumps during the expansion process and the post-spreading magmatic disturbances. The long-wavelength magnetic anomalies indicate lithospheric fractures and Curie surface variations in the SCS, which are affected by the post-spreading magmatic rejuvenation. The magnetic anomalies of the SCS resulted from the superposition of magnetic anomalies in the ocean crust and the uppermost mantle.

Keywords: spreading magnetic anomalies; nested elliptical directional filter; South China Sea; expansion process; interactions of plates; post-spreading magmatic rejuvenation

Citation: Wang, M.; Chen, S.; Gui, H. Spreading Magnetic Anomalies Separation of the South China Sea Based on the Nested Elliptical Directional Filters. *J. Mar. Sci. Eng.* **2023**, *11*, 521. https://doi.org/10.3390/jmse11030521

Academic Editor: Dimitris Sakellariou

Received: 24 January 2023
Revised: 23 February 2023
Accepted: 27 February 2023
Published: 27 February 2023

1. Introduction

Spreading magnetic anomalies recorded the paleo-geomagnetic field variation through the seafloor spreading process of ocean basins [1–3]. The symmetrical lineated magnetic anomalies distributed on both sides of the ocean ridges are evidence of seafloor spreading [1]. An accurate interpretation of spreading magnetic anomalies is the key to deciphering the detailed formation process of ocean basins [2–6]; for example, investigating the rotation and spreading history of the West Philippine Basin [7], evaluating the magnetic structure of the ocean crust [8], and determining of the age of the seafloor of the world's ocean basins [9,10]. Compared with typical oceanic basins (e.g., the Pacific and Atlantic oceans), the marginal sea basins have more intricate magnetic anomalies due to the complex tectonic settings, such as the South China Sea (SCS). The SCS is situated at the junction of the Philippine Sea, Eurasian, and Indo-Australian plates. The tectonic movements of the surrounding plates play a crucial role in the expansion of the SCS [11]. The formation process of the South China Sea included a complete Wilson cycle, the northwest compression of the Pacific plate in the Mesozoic, the rift extension in the early Cenozoic, the seafloor spreading from Oligocene to middle Miocene, and the arc–continent collision after the spreading [12]. The expansion mechanism of the SCS has always been a hot topic in geological oceanography [13].

Seamounts of different ages are widely distributed on the rugged seafloor of the SCS. The tectonic interaction between the seafloor and continent and the deep thermal structure of the oceanic lithosphere are potential factors affecting the seafloor spreading process of

the SCS. The spreading magnetic anomalies result from the thermoremanent magnetization of the ocean crust. They preserve the strength and direction of the paleo-geomagnetic field polarity reversals [14]. The spreading magnetic anomalies are an accurate record of the formation process of the ocean crust [1,15–23]. The interpretation of the spreading magnetic anomalies can shed light on the detailed expansion process of the SCS. However, the spreading magnetic anomalies of the SCS are inevitably disturbed by magmatic activities during or after the seafloor spreading, tectonic movement, and fluctuations in the Curie surface [4,5]. The SCS has experienced persistent and complex magmatic activities, and the magmatic evolution spans the extension of the SCS [24–31]. Pre-spreading magmatic activities mainly focus on the northern continental margin of the SCS and the coastal areas [32–34]. During expansion, magmatism is concentrated on the seafloor of SCS, and the oceanic crust is formed [35]. After the seafloor spreading, the magmatism is still active, forming many seamounts and intrusions [27,36]. The seamounts and intrusions usually result in short-wavelength disturbances, and the deep magnetic structures, for example, the fluctuations in the Curie surface, can result in long-wavelength magnetic anomalies [5,37]. The observed magnetic anomalies of the SCS superimpose the shallow and deep magnetic disturbances [35]. Previous studies have determined the age of the lineated magnetic anomalies of the SCS in the range of 33~15 Ma. However, the formation process of the lineated magnetic anomalies and the detailed evolutionary history of the SCS is still ambiguous [15–20]. Therefore, it is of great significance to separate the spreading magnetic anomalies and suppress the interference components to investigate the expansion process of the SCS.

Wang et al. [5] proposed the elliptical directional filter, which effectively suppresses the short-wavelength anomalies of magmatic disturbances. In this study, we propose nested elliptical directional filters to separate the spreading magnetic anomalies and suppress the short- and long-wavelength disturbances of the SCS. The separated spreading magnetic anomalies are of great significance when investigating the origin of the lineated magnetic anomalies and the expansion process of the SCS.

2. Materials and Methods

2.1. Geologic Setting

The SCS is located at the junction of the Philippine Sea, Eurasian, and Indo-Australian plates. The SCS is a rhomb-shaped marginal sea basin (Figure 1) formed during the Cenozoic era [38,39]. The continental rifting initiated along the southern margin of South China since the Eocene [40]; then, seafloor spreading started from the northwestern sub-basin (NWSB) and eastern sub-basin (ESB) and propagated to the southwestern sub-basin (SWSB) [30]. The NWSB is the smallest sub-basin of the SCS, and it is the first to expand. The water depth of the NWSB is 2700~3900 m. The spreading age of the NWSB is in the range of 33~23 Ma [17]. The ESB is the largest sub-basin of the SCS, and the water depth of the ESB is 1000~5000 m. The spreading age of the ESB is in the range of 32~15 Ma [18,20]. The SWSB is formed by the expansion of the SCS at the latest stage. The spreading age of the SWSB is in the range of 24~15 Ma [3,18,40,41]. The water depth of the SWSB is 3000~4800 m. During seafloor spreading, ridge jumps occurred, resulting in the asymmetric geometry of the ESB [20,33]. The accretion of the oceanic crust was asymmetric in the ESB, and the northern flank is larger than the southern one. The sediment thickness of the South China Sea basin is in the range of 0~2000 m, and igneous intrusions are widely distributed under the sedimentary layer [42]. Seamounts of different heights and sizes are prevalently distributed on the seafloor of the SCS. Most of the seamounts were formed by magmatic activities after the cessation of the seafloor spreading [29]. The widespread magmatic activities were suggested to be induced by extension due to the cooling and subsidence of the oceanic lithosphere and plate interactions [29,32].

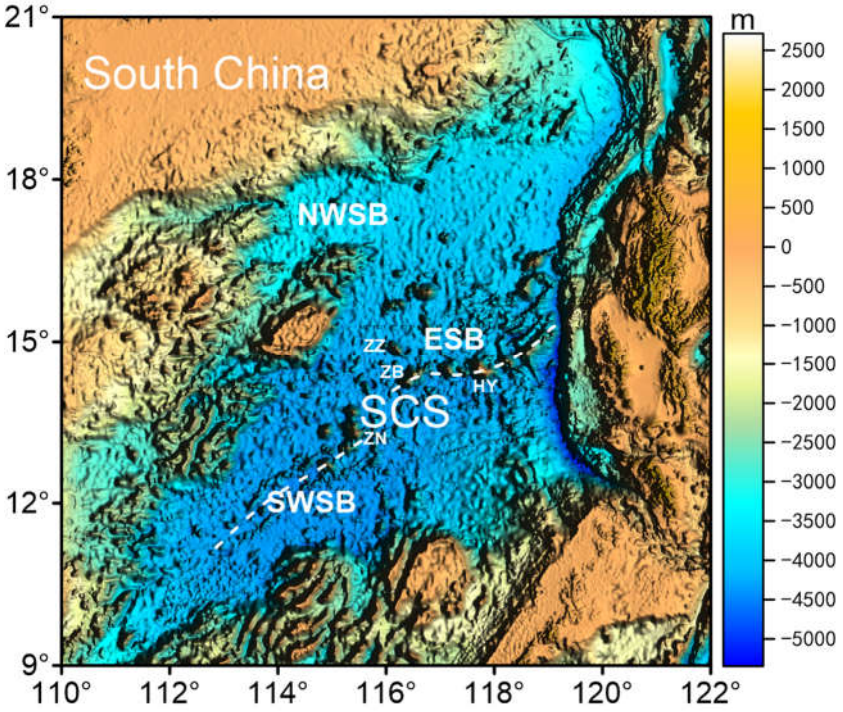

Figure 1. The topography of the South China Sea. ESB, eastern sub-basin of the SCS; NWSB, northwestern sub-basin of the SCS; SWSB, southwestern sub-basin of the SCS; ZZ, Zhangzhong seamount; ZB, Zhenbei seamount; ZN, Zhongnan seamount; HY, Huangyan seamount. The dashed white line denotes the fossil spreading ridge. The topographic data are derived from the General Bathymetric Chart of the Oceans (GEBCO).

2.2. Magnetic Anomalies of the SCS

The magnetic anomalies of the SCS are roughly striped (Figure 2). Although these magnetic anomalies are believed to be formed by seafloor spreading, they are different from the spreading magnetic anomalies of the typical ocean basins. The fossil spreading ridges of the ESB and SWSB are not continuous, and the offset is nearly 100 km [43]. The fossil spreading ridge of the SWSB is close to a straight line, while, for the ESB, the fossil spreading ridge is not linear but has a barbed shape. Specifically, the trend of the magnetic anomaly stripes is not strictly parallel to the fossil spreading ridge, and the magnetic lineations of the SCS are distorted and discontinuous. The expansion of the NWSB, ESB, and SWSB has different characteristics [44]. The magnitude of the magnetic anomalies of the NWSB, ESB, and SWSB is in the range of −150~230 nT (nanotesla), −440~460 nT, and −190~200 nT, respectively. The magnetic anomalies of the SCS are relatively clear in the ESB with a high amplitude, while the magnetic anomalies of the NWSB and SWSB have a weak amplitude, and the age of the magnetic lineations is difficult to identify. Ben-Avraham and Uyeda [45] were the first to point out that there are EW-lineated magnetic anomalies in the SCS. Then, Taylor and Hayes [16] interpreted these lineated magnetic anomalies as a reflection of seafloor spreading. They suggested that the seafloor spreading occurred in the Middle Oligocene to Early Miocene. According to magnetic surveys and ocean drillings, the time of seafloor spreading of the SCS is in the range of 33~15 Ma, and the full spreading rate varies in the range of 40~80 km/Ma [16–18,20]. The trend in the lineated magnetic anomalies of the SCS can be roughly divided into two groups: northeast in the SWSB and near east–west in the ESB and NWSB. Specifically, the strike of the magnetic anomalies of the SWSB is between 50°and 70°, and the ESB and NWSB are between 80°and 100°. Post-spreading magmatic activities are prevalent, and the magnetic anomalies of seamounts and intrusions introduce significant interferences to the spreading magnetic lineations [19,32,36].

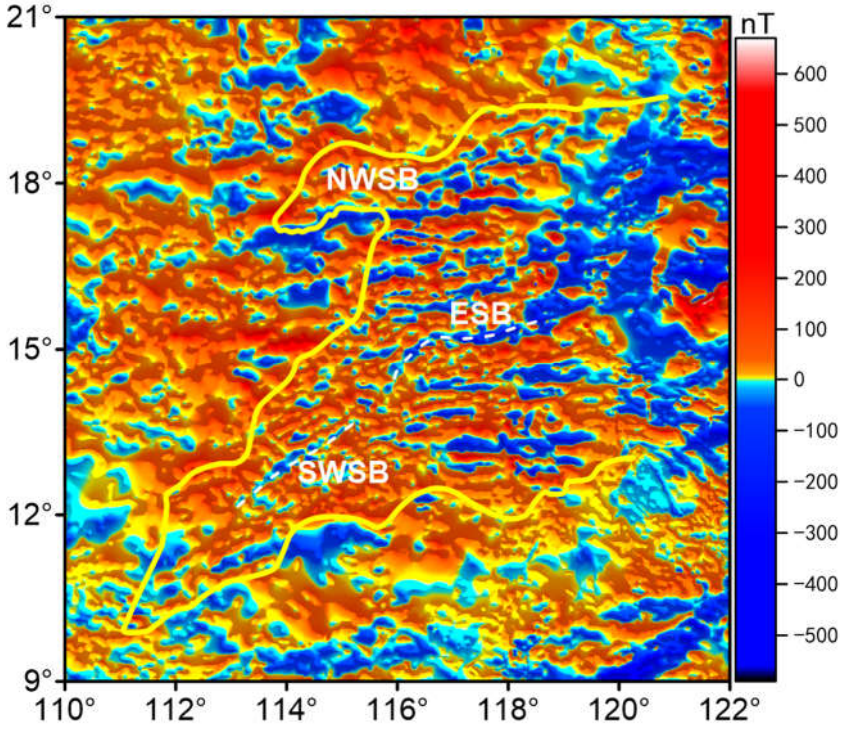

Figure 2. The magnetic anomalies of the South China Sea. The dashed white line denotes the position of the fossil spreading ridge. The solid yellow line denotes the continent-ocean boundary [35]. The magnetic anomaly data are from the Coordinating Committee for Geoscience Programs in East and Southeast Asia (CCOP).

2.3. Nested Elliptical Directional Filters

The observed magnetic anomalies are the superposition of magnetic sources of shallow and deep magnetic structures. Seamounts and intrusions are shallow magnetic bodies and mainly result in short-wavelength magnetic disturbances [5]. Magnetic anomalies induced by deep magnetic structures (e.g., fluctuations in the Curie surface) are mainly long-wavelength anomalies [35]. Wang et al. [5,46] proved that the spectrum of the spreading magnetic anomalies is mainly distributed in the direction perpendicular to the lineations in the frequency domain. Furthermore, the interference anomalies are usually randomly distributed, with an isotropic spectrum in the frequency domain. Therefore, we aimed to preserve the main frequency components of the spreading magnetic anomalies and cut off the high- and low-frequency components to suppress interference anomalies as much as possible. Thus, we propose using nested elliptical directional filters to separate the spreading magnetic anomalies. The nested elliptical directional filters are composed of two elliptical directional filters with different widths in the major and minor axes.

Let f_{a}, f_{b} represent the frequency response of two elliptical directional filters with different widths in the major axis and the minor axis. In the frequency domain, the f_{a} and f_{b} filters were denoted as:

$$f_{\mathrm{a}}(u,v) = \begin{cases} \frac{1}{2}[1+\cos\alpha] & (\alpha < \pi) \\ 0 & (\alpha \geq \pi) \end{cases}, \; f_{\mathrm{b}}(u,v) = \begin{cases} \frac{1}{2}[1+\cos\beta] & (\beta < \pi) \\ 0 & (\beta \geq \pi) \end{cases} \tag{1}$$

where $\alpha = \left[\frac{u^2}{\Delta u_a^2} + \frac{v^2}{\Delta v_a^2}\right]^{1/2} \cdot \pi$, $\beta = \left[\frac{u^2}{\Delta u_b^2} + \frac{v^2}{\Delta v_b^2}\right]^{1/2} \cdot \pi$, $\Delta u_a, \Delta u_b$ are the half-widths of the major axis of the f_{a} and f_{b}, respectively, $\Delta v_a, \Delta v_b$ are the half-widths of the minor axis of the f_{a} and f_{b}, respectively, and $\Delta u_a > \Delta u_b$ and $\Delta v_a > \Delta v_b$, u, v are the wavenumbers in the

x and y axis directions, respectively. The direction of the major axis of the f_a and f_b filters can be changed by the coordinate rotation transformation as follows:

$$\begin{cases} u' = u\cos\alpha - v\sin\alpha \\ v' = v\cos\alpha + u\sin\alpha \end{cases} \quad (2)$$

where u', v' are the wavenumbers of the transformed coordinates in the x and y axis direction, respectively; u, v are the wavenumbers of the original coordinates in the x and y axis direction, respectively; α is the counter-clockwise rotation angle from the original to the new coordinate.

The filtering process of the nested elliptical directional filters can be divided into three steps. First, the observed magnetic anomalies are filtered by the f_a filter (Figure 3a) to suppress the short-wavelength disturbances, and the filtered magnetic anomalies are denoted as FM_a. The FM_a contains the spreading magnetic anomalies and long-wavelength disturbances. Then, the f_b filter (Figure 3b) is used to filter the observed magnetic anomalies to derive the long-wavelength disturbances, and the filtered magnetic anomalies are presented as FM_b. Finally, the separated magnetic anomalies are obtained by subtracting FM_b from FM_a. Figure 3a,b show the responses of the f_a and f_b filters, where $\Delta u_a = 1.0$ rad/km, $\Delta v_a = 0.5$ rad/km, $\Delta u_b = 0.2$ rad/km, and $\Delta v_b = 0.1$ rad/km. Figure 3c,d show the response of the f_a and f_b filters in the direction of the major axis and minor axis, respectively. This shows that the f_a and f_b filters are anisotropic low-pass filters with different pass-band widths in the direction of the major and minor axes.

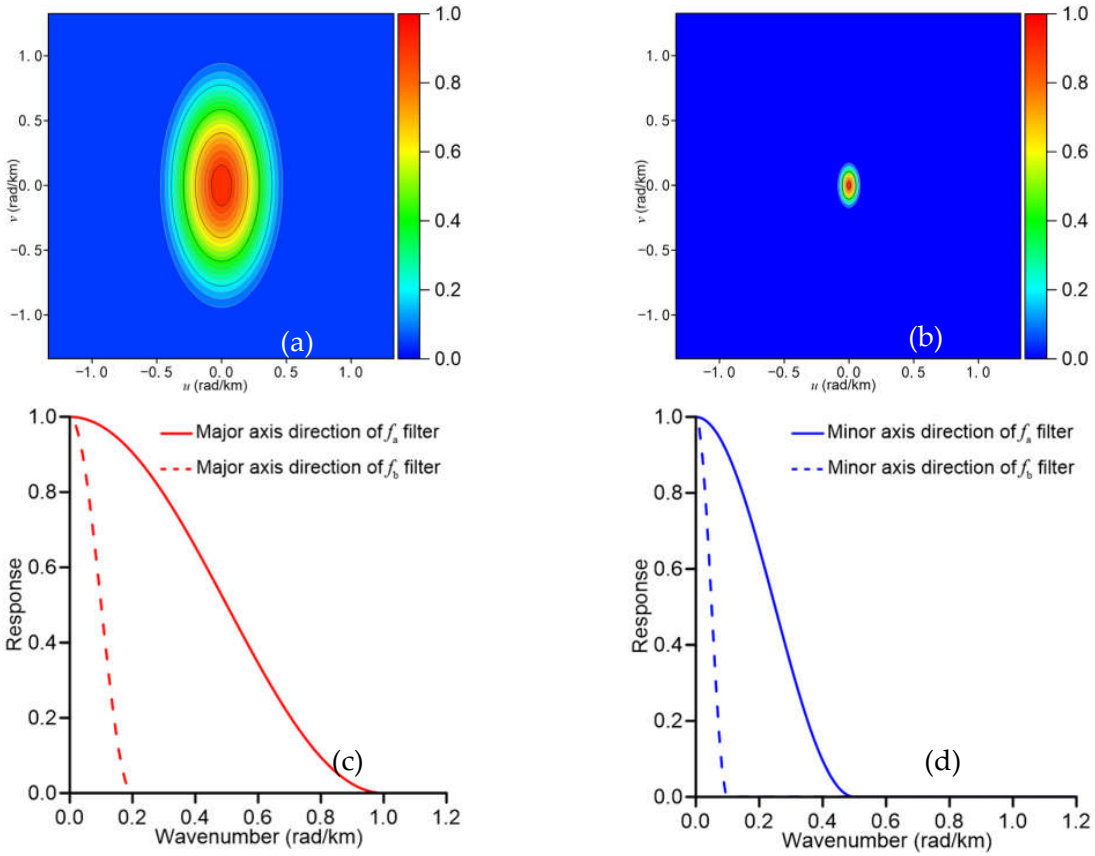

Figure 3. The responses of the f_a and f_b filters. (**a**) The response of the f_a filter. (**b**) The response of the f_b filter. (**c**) The response of the f_a and f_b filters in the direction of the major axis. The solid red line and the dashed red line denote the response of the f_a and f_b filters in the direction of the major axis, respectively. (**d**) The response of the f_a and f_b filters in the direction of the minor axis. The solid blue line and the dashed blue line denote the response of the f_a and f_b filters in the direction of the minor axis, respectively.

3. Results

3.1. The Nested Elliptical Directional Filters of the SCS

The logarithmic power spectrum of the magnetic anomalies of the SCS is shown in Figure 4. This shows that the spectrum of the SCS is anisotropic, with the major response approximately perpendicular to the lineated magnetic anomalies. The strikes of the magnetic anomalies of the SCS are in the range of 50°~100°. Since the frequency response of the spreading magnetic anomalies is perpendicular to the strike of the lineation [5,46], we set the major axis of the f_{a} and f_{b} filters in the azimuth of 170°. The parameters of the nested elliptical directional filters were obtained after many experiments. The half-width of the major and minor axes of the f_{a} filter are $\Delta u_a = 1.2$ rad/km and $\Delta v_a = 0.5$ rad/km, respectively, and the half-width of the major and minor axes of the f_{b} filter are $\Delta u_b = 0.3$ rad/km and $\Delta v_b = 0.2$ rad/km, respectively (Figure 5a,b). Figure 5c,d shows the response of the f_{a} and f_{b} filters in the directions of the major and minor axes, respectively. The f_{a} and f_{b} filters take advantage of the anisotropic frequency response of the spreading magnetic anomalies. The nested elliptical directional filters suppress the short- and long-wavelength disturbances with varying pass-band widths in different directions. Two filtering effects are shown; first, short-wavelength and long-wavelength disturbances are suppressed in different directions. Second, the pass-band width is anisotropic and broad in the direction of the major axis and narrow in the direction of the minor axis; thus, it can preserve the frequency components of the spreading magnetic anomalies as much as possible.

3.2. The Separated Spreading Magnetic Anomalies of the SCS

The separated spreading magnetic anomalies of the SCS are shown in Figure 6. Figure 6a shows the filtered magnetic anomalies of the SCS using the f_{a} filter. We can see that the short-wavelength disturbances are significantly suppressed, and the lineation is clearer than before (Figure 2). However, the filtered magnetic anomalies still contain long-wavelength disturbances induced by deep magnetic structures. Therefore, we filter the magnetic anomalies of the SCS using the f_{b} filter to derive the long-wavelength components. Figure 6b shows the filtered magnetic anomalies of the SCS by the f_{b} filter. The filtered magnetic anomalies by the f_{b} filter show broad and banded long-wavelength anomalies in which the positive magnetic anomalies dominate. The banded magnetic anomalies are broad and continuous in the ESB and SWSB, respectively. The NWSB is dominated by positive anomalies trending nearly east to west. These long-wavelength magnetic anomalies reflect the oceanic crust's deep magnetic structures. The separated spreading magnetic anomalies of the SCS by the nested elliptical directional filters are shown in Figure 6c. The separated magnetic anomalies are derived from f_{a} filtered magnetic anomalies subtracting f_{b} filtered magnetic anomalies. This shows that the disturbances of short- and long-wavelength magnetic anomalies are effectively suppressed, and the texture of the spreading magnetic anomalies is clearer. The fossil spreading ridges of ESB and SWSB correspond to the negative magnetic anomalies, and they are discontinuous, with an offset in the north–south direction. The fossil spreading ridge of the NWSB is difficult to identify because there are no significant symmetrical magnetic lineations. The spreading magnetic anomalies of the SCS are complex and different from the typical ocean basins. The spreading magnetic anomalies are warped, interrupted, and not strictly parallel to each other. This may reflect the intermittency of magma eruptions and the movement of the spreading ridge axis during the spreading process. In addition, the post-spreading magmatic activities are another potential factor.

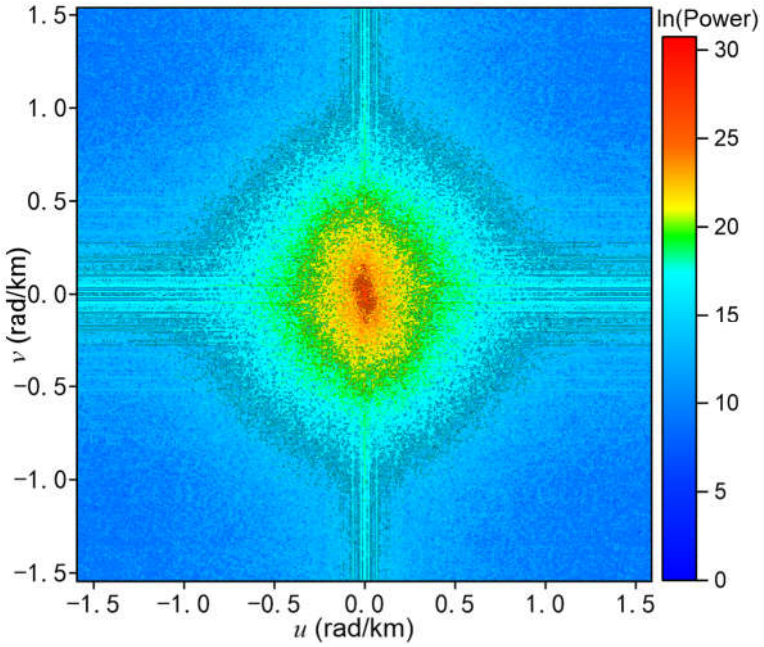

Figure 4. The logarithmic power spectrum of the magnetic anomalies of the SCS.

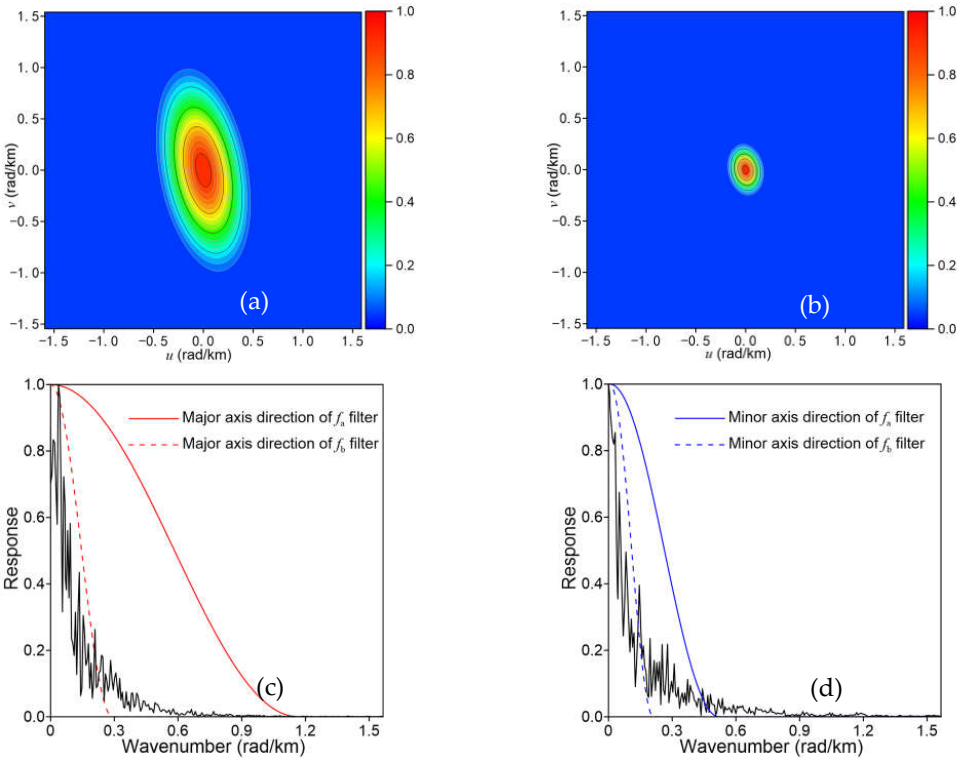

Figure 5. The response of the f_a and f_b filters. (**a**) The response of the f_a filter. (**b**) The response of the f_b filter. (**c**) The response of the f_a and f_b filter in the direction of the major axis. The solid red line and the dashed red line represent the response of the f_a and f_b filters in the direction of the major axis, respectively. The solid black line represents the normalized amplitude spectrum of the magnetic anomalies of the SCS in the direction of the major axis. (**d**) The response of the f_a and f_b filters in the direction of the minor axis. The solid blue line and the dashed blue line represent the response of the f_a and f_b filters in the direction of the minor axis, respectively. The solid black line represents the normalized amplitude spectrum of the magnetic anomalies of the SCS in the direction of the minor axis.

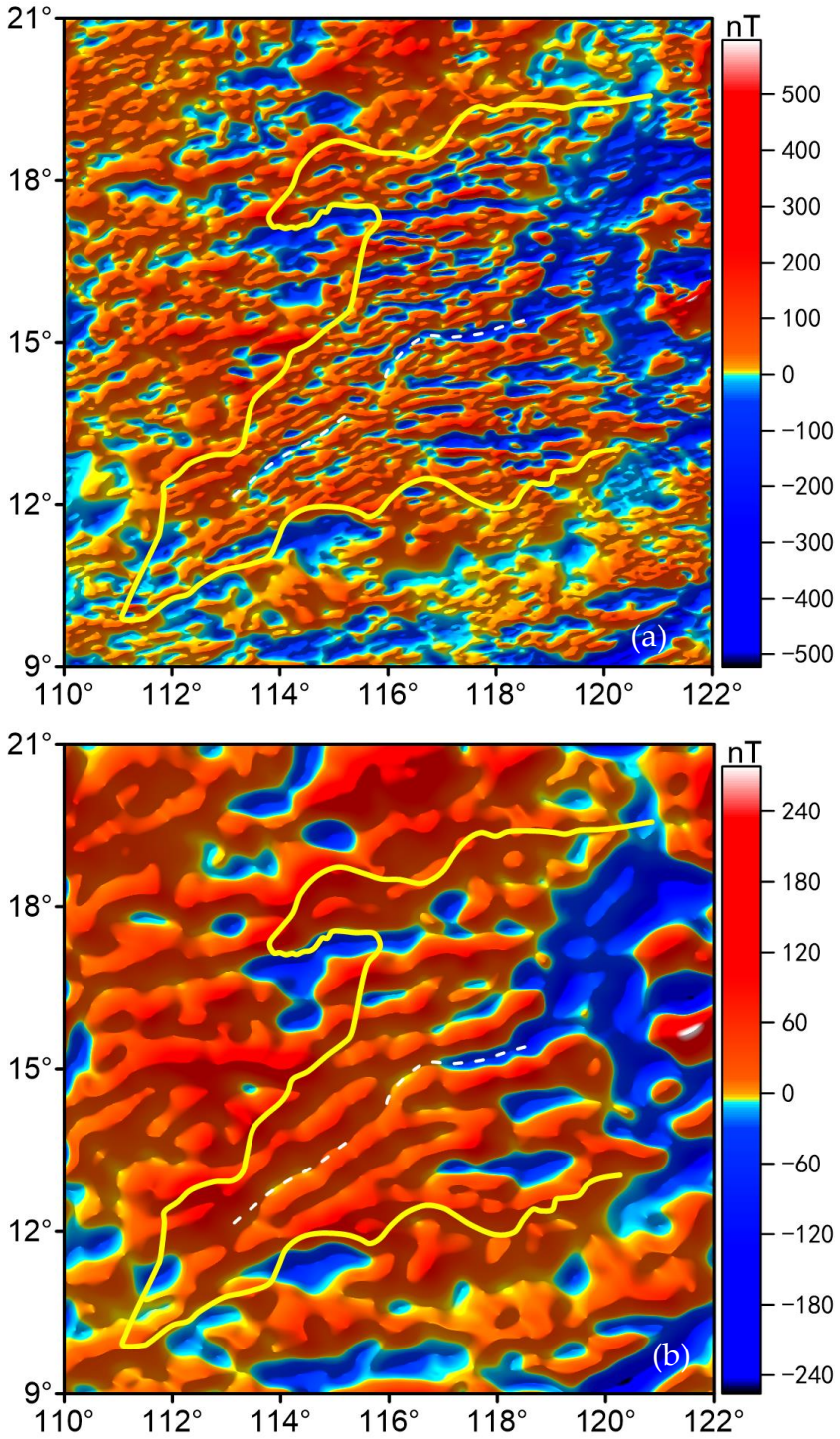

Figure 6. *Cont.*

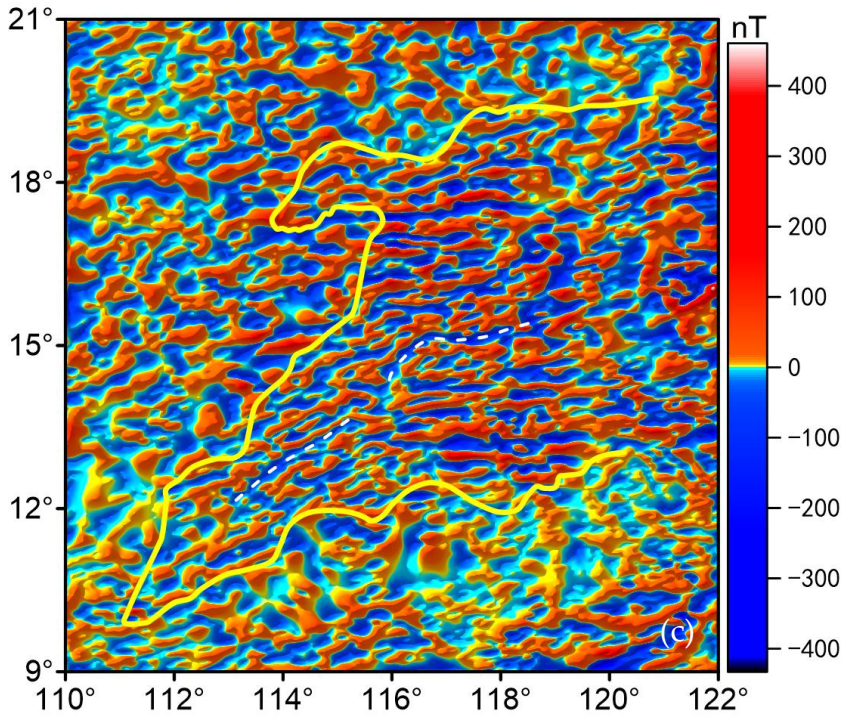

Figure 6. Separation results from the magnetic anomalies of the SCS. (**a**) The f_a filtered magnetic anomalies. (**b**) The f_b filtered magnetic anomalies (**c**) The separated spreading magnetic anomalies of the SCS by the nested elliptical directional filters. The solid yellow line denotes the continent–ocean boundary. The dashed white line denotes the position of the fossil spreading ridge.

4. Discussion

4.1. The Pattern of the Spreading Magnetic Anomalies of the SCS

The seafloor expansion of the SCS is under complex tectonic environments [47–51]. The SCS is a plate-edge-type rifting basin located at the junction of the Philippine Sea, Eurasian, and Indo-Australian plates [12]. The SCS underwent continental rifting, seafloor spreading, and eastward subduction under the Philippine Sea plate [16–18,33,44,49]. The interactions of the surrounding plates affect the expansion process of the SCS [12]. The separated spreading magnetic anomalies recorded the expansion details of the SCS. The fossil spreading ridge of the ESB has a barb shape. However, except for the negative anomalies at the fossil ridge and the positive anomalies on both flanks, the strike of the spreading magnetic anomalies of the ESB is not strictly parallel to the fossil spreading ridge. The barb shape may indicate that the ESB caused a rotation in the final stage of the seafloor spreading. The irregular magnetic anomalies reflect that the shape and position of the spreading ridge are changing during seafloor expansion. The spreading rate of the SCS varied greatly during expansion. The full spreading rate of the SCS is in the range of 20~80 km/Ma. The spreading rate is relatively high in the early stage of seafloor spreading, then decreases to an average of 25 km/Ma during 26~29 Ma. After that, the full spreading rate reaches a 70 km/Ma peak during 23.6~26 Ma, then drops to a low spreading rate of 50~35 km/Ma until the end of the seafloor spreading [18]. The large variations in the spreading rate may have affected the stability of the spreading ridge. The magnetic lineations of the SCS are forked, discontinuous and interlaced (Figure 6c). The pattern of the spreading magnetic anomalies indicates that the formation process of the SCS is very complex, and should be affected by surrounding plate motions. Many studies have been carried out on the spreading dynamics of the SCS, such as active spreading, passive spreading, mantle convection, subduction and drag, and collision extrusion models have been proposed [16,17,49–51]. During expansion, ridge reorientation frequently occurs in the SCS, which adapts to the direction changes in surrounding plate motion [17]. The

spreading ridge occurred ridge jump many times throughout the spreading process, at different positions on the ocean basin [20,21]. Notably, volcanic activities near and off the fossil spreading ridge are prevalent after the seafloor spreading in the SCS [52]. These magmatic activities mainly occurred between approximately 3 and 11 Ma in the Later Miocene [27–30,53], for example, the Zhangzhong Seamount, Huangyan Seamount, Zhenbei Seamount, and Zhongnan Seamount (Table 1). The expansion of the SCS lasted for a relatively short time [54]. However, the spreading ridge migrated several times, and the magmatic activities were prolonged after the cessation of expansion. The movement of the surrounding plates plays a crucial role in the expansion of the SCS and influences the pattern of the spreading magnetic anomalies. According to multi-channel seismic data of the northern ridge flanks of the SCS, at least two southward ridge jumps happened at around 23.6 Ma and 27 Ma [33], respectively. The spreading magnetic anomalies are forky and discontinuous, and the lineation is not strictly parallel. The spreading magnetic anomalies of the SCS were significantly affected by the post-spreading magmatic activities and the ridge jumps during the expansion process. The effects of plate motions and magmatic activities should be considered in the interpretation of the complex magnetic anomalies of the SCS.

Table 1. The age of SCS seamounts.

Seamount	Zhangzhong	Huangyan	Zhenbei	Zhongnan
Location	116.185° E, 15.5683° N	117.768° E, 15.170° N	116.461° E, 15.014° N	115.410° E, 14.009° N
Age	4.76-5.78 Ma	7.28~8.26 Ma	8.5~11.3 Ma	2.91~4.07 Ma
References	Yan et al., 2008 [27]; Jiang et al., 2019 [29]	Wang et al., 2009 [25]	Wang and Wu, 1985 [24]	Yang et al., 2011 [28]; Jiang et al., 2019 [29]

4.2. Source of the Magnetic Anomalies of the SCS

The observed magnetic anomalies in the SCS were induced by the superposition of magnetic anomalies in the shallow and deep magnetic structures. The basement of the SCS is rough, and igneous intrusions and seamounts are well-developed [33]. The crust of the SCS is the oceanic crust, and the crust thickness of the SCS is 5–8 km [53]. Generally, the oceanic crust can be divided into the basalt, dike, and gabbro layers, from top to bottom. The basalt layer is regarded as the primary contributor to the spread of magnetic anomalies because it has a strong remanent magnetization and is located on the upper part of the oceanic crust. However, the dike and gabbro layers have moderate magnetization in the deep oceanic crust; sometimes, even the uppermost mantle is an also essential source of magnetic anomalies [8,55,56]. The deep magnetic structure can significantly influence the shape of the observed magnetic anomalies; for example, the fluctuations in the Curie surface can cause long-wavelength anomalies. The separated spreading magnetic anomalies caused by the nested elliptical directional filters mainly result from the oceanic crust, showing the expansion process of the SCS (Figure 6c). The broad and banded long-wavelength magnetic anomalies (Figure 6b) may indicate lithospheric fractures and Curie surface variations affected by the rejuvenation of magmatic activities. The prevalent post-spreading magmatism along and off the fossil spreading ridge shows the expression of the rejuvenation of magmatic activity [33], and is an essential factor modifying the fluctuations in the Curie surface. Li et al. [56] suggested that the Curie depth of the central basin of the SCS is beneath the Moho, and nearly 10 km of the uppermost mantle is magnetized. The long-wavelength magnetic anomalies indicate that the magnetic anomalies of the SCS resulted from the superposition of magnetic anomalies in the ocean crust and the uppermost mantle. The magnetic anomalies in the SCS are disturbed by magmatic activities, tectonic movement, and Curie surface fluctuations. Therefore, the

distribution of the magnetic lineations is more complicated under the effects of the shallow and deep magnetic structures.

5. Conclusions

The SCS is situated at the junction of the Philippine sea, Eurasian, and Indo-Australian plates. The movement of the surrounding plates plays a crucial role in the expansion of the SCS and influences the pattern of the spreading magnetic anomalies. The nested elliptical directional filters effectively suppress the short- and long-wavelength interference magnetic anomalies. The spreading magnetic anomalies separated by the nested elliptical directional filters depict the expansion process of the SCS. The spreading magnetic anomalies of the SCS are warped, interrupted, and not strictly parallel to each other. The pattern of the spreading magnetic anomalies reflects the post-spreading magmatic interferences and multiple ridge jumps during the expansion process. The long-wavelength magnetic anomalies indicate lithospheric fractures and Curie surface variationa in the SCS, which are affected by the post-spreading magmatic rejuvenation. The magnetic anomalies of the SCS resulted from the superposition of magnetic anomalies in the ocean crust and the uppermost mantle.

Author Contributions: Conceptualization, methodology, and writing—original draft preparation, M.W.; validation, S.C.; supervision and writing—review and editing, H.G.; All authors have read and agreed to the published version of the manuscript.

Funding: This research was funded by the Postdoctoral Research Start Fund Project (Grant Number 2022BSH002), Scientific Research Platform Project of Suzhou University (Grant Number 2021XJPT54), and Natural Science Projects of Colleges and Universities in Anhui Province (Grant Number 2022AH051387).

Institutional Review Board Statement: Not applicable.

Informed Consent Statement: Not applicable.

Data Availability Statement: The data used in this study are available on request from the corresponding author.

Acknowledgments: The authors would like to thank the reviewers' suggestions. This research is supported by the Postdoctoral Research Start Fund Project (Grant Number 2022BSH002), Scientific Research Platform Project of Suzhou University (Grant Number 2021XJPT54), and Natural Science Projects of Colleges and Universities in Anhui Province (Grant Number 2022AH051387).

Conflicts of Interest: The authors declare no conflict of interest.

References

1. Vine, F.J.; Matthews, D.H. Magnetic anomalies over oceanic ridges. *Nature* **1963**, *199*, 947–949. [CrossRef]
2. Choe, H.; Dyment, J. The fate of marine magnetic anomaly in subduction zones: A global appraisal. *Earth Planet. Sci. Lett.* **2021**, *561*, 116787. [CrossRef]
3. Qiu, N.; Sun, Z.; Lin, J.; Li, C.F.; Xu, X. Dating seafloor spreading of the southwest sub-basin in the South China Sea. *Gondwana Res.* **2022**. [CrossRef]
4. Wang, M.M.; Cao, J. An automatic identification method of marine magnetic anomalies based on the sliding window correlation coefficient method. *J. Appl. Geophys.* **2022**, *205*, 104761. [CrossRef]
5. Wang, M.M.; Cao, J.; Li, J.L.; Liu, X.H. Extraction of Marine Magnetic Anomalies under Magmatic Disturbances Based on an Anisotropic Elliptical Directional Filter. *Pure Appl. Geophys.* **2022**, *179*, 2289–2309. [CrossRef]
6. Wang, M.M.; Cao, J.; Li, J.L.; Liu, X.H. Identification of marine magnetic anomalies based on the sliding window curve similarity method. *Earth Planets Space* **2022**, *74*, 79. [CrossRef]
7. Sasaki, T.; Yamazaki, T.; Ishizuka, O. A revised spreading model of the West Philippine Basin. *Earth Planets Space* **2014**, *66*, 83. [CrossRef]
8. Dyment, J.; Arkani-Hamed, J.; Ghods, A. Contribution of serpentinized ultramafics to marine magnetic anomalies at slow and intermediate spreading centres: Insights from the shape of the anomalies. *Geophys. J. Int.* **1997**, *129*, 691–701. [CrossRef]
9. Müller, R.D.; Sdrolias, M.; Gaina, C.; Roest, W.R. Age, spreading rates, and spreading asymmetry of the world's ocean crust. *Geochem. Geophys. Geosystems* **2008**, *9*, 1–19. [CrossRef]
10. Seton, M.; Müller, R.D.; Zahirovic, S.; Williams, S.; Wright, N.M.; Cannon, J.; Whittaker, J.M.; Matthews, K.J.; McGirr, R. A global data set of present-day oceanic crustal age and seafloor spreading parameters. *Geochem. Geophys. Geosystems* **2020**, *21*, e2020GC009214. [CrossRef]

11. Morley, C.K. Major unconformities/termination of extension events and associated surfaces in the South China Seas: Review and implications for tectonic development. *J. Asian Earth Sci.* **2016**, *120*, 62–86. [CrossRef]
12. Wang, P.; Huang, C.; Lin, J.; Jian, Z.; Sun, Z.; Zhao, M. The South China Sea is not a mini-Atlantic: Plate-edge rifting vs intra-plate rifting. *Natl. Sci. Rev.* **2019**, *6*, 902–913. [CrossRef] [PubMed]
13. Qiu, Y.; Huang, W.; Wei, J.; Han, B.; Xie, Z.; Du, W. Spreading pattern with scissors of Southwest sub-basin in the South China Sea (in Chinese). *Acta Geol. Sin.* **2022**, *96*, 2743–2760.
14. Dyment, J.; Arkani-Hamed, J. Spreading-rate-dependent magnetization of the oceanic lithosphere inferred from the anomalous skewness of marine magnetic anomalies. *Geophys. J. Int.* **1995**, *121*, 789–804. [CrossRef]
15. Taylor, B.; Hayes, D.E. The tectonic evolution of the South China Basin. *Wash. DC Am. Geophys. Union Geophys. Monogr. Ser.* **1980**, *23*, 89–104. [CrossRef]
16. Taylor, B.; Hayes, D.E. Origin and history of the South China Sea basin. *Wash. DC Am. Geophys. Union Geophys. Monogr. Ser.* **1983**, *27*, 23–56. [CrossRef]
17. Briais, A.; Patriat, P.; Tapponnier, P. Updated interpretation of magnetic anomalies and seafloor spreading stages in the South China Sea: Implications for the Tertiary tectonics of Southeast Asia. *J. Geophys. Res. Solid Earth* **1993**, *98*, 6299–6328. [CrossRef]
18. Li, C.F.; Xu, X.; Lin, J.; Sun, Z.; Zhu, J.; Yao, Y.; Zhao, X.; Liu, Q.; Kulhanek, D.K.; Wang, J.; et al. Ages and magnetic structures of the South China Sea constrained by deep tow magnetic surveys and IODP Expedition 349. *Geochem. Geophys. Geosystems* **2014**, *15*, 4958–4983. [CrossRef]
19. Zahirovic, S.; Seton, M.; Müller, R.D. The cretaceous and cenozoic tectonic evolution of Southeast Asia. *Solid Earth* **2014**, *5*, 227–273. [CrossRef]
20. Guan, Q.; Zhang, T.; Taylor, B.; Gao, J.; Li, J. Ridge jump reorientation of the South China Sea revealed by high-resolution magnetic data. *Terra Nova* **2021**, *33*, 475–482. [CrossRef]
21. Dyment, J. Evolution of the Carlsberg Ridge between 60 and 45 Ma: Ridge propagation, spreading asymmetry, and the Deccan-Reunion hotspot. *J. Geophys. Res. Solid Earth* **1998**, *103*, 24067–24084. [CrossRef]
22. Granot, R.; Dyment, J. The Cretaceous opening of the South Atlantic Ocean. *Earth Planet. Sci. Lett.* **2015**, *414*, 156–163. [CrossRef]
23. Gürer, D.; Granot, R.; van Hinsbergen, D.J.J. Plate tectonic chain reaction revealed by noise in the Cretaceous quiet zone. *Nat. Geosci.* **2022**, *15*, 233–239. [CrossRef]
24. Wang, X.J.; Wu, M.Q.; Liang, D.H.; Yin, A.W. Some geochemical characteristics of basalts in the South China Sea. *Acta Geochim.* **1985**, *4*, 380–390. [CrossRef]
25. Wang, Y.J.; Han, X.Q.; Luo, Z.H.; Qiu, Z.Y.; Ding, W.W.; Li, J.B.; Gao, S.T.; Chen, R.H. Late Miocene magmatism and evolution of Zhenbei-Huangyan Seamount in the South China Sea: Evidence from petrochemistry and chronology (in Chinese). *Acta Oceanol. Sin.* **2009**, *31*, 93–102.
26. Yan, P.; Deng, H.; Liu, H.; Zhang, Z.; Jiang, Y. The temporal and spatial distribution of volcanism in the South China Sea region. *J. Asian Earth Sci.* **2006**, *27*, 647–659. [CrossRef]
27. Yan, Q.; Shi, X.; Wang, K.; Bu, W.; Xiao, L. Major element, trace element, and Sr, Nd and Pb isotope studies of Cenozoic basalts from the South China Sea. *Sci. China Ser. D Earth Sci.* **2008**, *51*, 550–566. [CrossRef]
28. Yang, S.Y.; Fang, N.Q.; Yang, S.X.; Yao, B.C.; Liang, D.H. A further discussion on formation background and tectonic constraints of igneous rocks in Central Sub-Basin of the South China Sea. *Earth Sci* **2011**, *36*, 455–470.
29. Jiang, T.; Gao, H.; He, J.; Tian, D. Post-spreading volcanism in the central South China Sea: Insights from zircon U–Pb dating on volcaniclastic breccia and seismic features. *Mar. Geophys. Res.* **2019**, *40*, 185–198. [CrossRef]
30. Yu, J.; Yan, P.; Qiu, Y.; Delescluse, M.; Huang, W.; Wang, Y. Oceanic crustal structures and temporal variations of magmatic budget during seafloor spreading in the East Sub-basin of the South China Sea. *Mar. Geol.* **2021**, *436*, 106475. [CrossRef]
31. Gao, J.; Wu, S.; Lüdmann, T.; Li, C.F.; Li, L.; Lu, Y.; Yang, Z.; Tian, L.; Qin, Y.; Song, T. Extensional structures and Cenozoic magmatism in the northwestern South China Sea. *Gondwana Res.* **2022**. [CrossRef]
32. Song, X.; Li, C.F.; Yao, Y.; Shi, H. Magmatism in the evolution of the South China Sea: Geophysical characterization. *Mar. Geol.* **2017**, *394*, 4–15. [CrossRef]
33. Ding, W.; Sun, Z.; Dadd, K.; Fang, Y.; Li, J. Structures within the oceanic crust of the central South China Sea basin and their implications for oceanic accretionary processes. *Earth Planet. Sci. Lett.* **2018**, *488*, 115–125. [CrossRef]
34. Zhu, S.; Yao, Y.; Li, X.; Gao, H.; Zhang, J.; Xu, Z.; Wang, J. Spatio-temperal distribution and mechenism of Cenozoic magmatism in the South China Sea and adjacent areas: Insight from seismic, geochemical and geochronological data. *Int. Geol. Rev.* **2022**, *64*, 2204–2231. [CrossRef]
35. Li, C.F.; Song, T.R. Magnetic recording of the Cenozoic oceanic crustal accretion and evolution of the South China Sea basin. *Chin. Sci. Bull.* **2012**, *57*, 3165–3181. [CrossRef]
36. Zhao, M.; He, E.; Sibuet, J.C.; Sun, L.; Qiu, X.; Tan, P.; Wang, J. Postseafloor spreading volcanism in the central east South China Sea and its formation through an extremely thin oceanic crust. *Geochem. Geophys. Geosystems* **2018**, *19*, 621–641. [CrossRef]
37. Li, C.F.; Wang, J.; Lin, J.; Wang, T. Thermal evolution of the North Atlantic lithosphere: New constraints from magnetic anomaly inversion with a fractal magnetization model. *Geochem. Geophys. Geosystems* **2013**, *14*, 5078–5105. [CrossRef]
38. Wang, P.; Li, S.; Suo, Y.; Guo, L.; Santosh, M.; Li, X.; Wang, G.; Jiang, Z.; Liu, B.; Zhou, J.; et al. Structural and kinematic analysis of Cenozoic rift basins in South China Sea: A synthesis. *Earth-Sci. Rev.* **2021**, *216*, 103522. [CrossRef]

39. Suo, Y.; Li, S.; Peng, G.; Du, X.; Zhou, J.; Wang, P.; Wang, G.; Somerville, I.; Diao, Y.; Liu, Z.; et al. Cenozoic basement-involved rifting of the northern South China Sea margin. *Gondwana Res.* **2022**. [CrossRef]
40. Burton-Johnson, A.; Cullen, A.B. Continental rifting in the South China Sea through extension and high heat flow: An extended history. *Gondwana Res.* **2022**. [CrossRef]
41. Barckhausen, U.; Roeser, H.A. Seafloor spreading anomalies in the South China Sea revisited. *Cont. -Ocean Interact. East Asian Marg. Seas* **2004**, *149*, 121–125. [CrossRef]
42. Braitenberg, C.; Wienecke, S.; Wang, Y. Basement structures from satellite-derived gravity field: South China Sea ridge. *J. Geophys. Res. Solid Earth* **2006**, *111*, 1–15. [CrossRef]
43. Ding, W.; Li, J. Propagated rifting in the Southwest Sub-basin, South China Sea: Insights from analogue modelling. *J. Geodyn.* **2016**, *100*, 71–86. [CrossRef]
44. Sibuet, J.C.; Yeh, Y.C.; Lee, C.S. Geodynamics of the south China sea. *Tectonophysics* **2016**, *692*, 98–119. [CrossRef]
45. Ben-Avraham, Z.; Uyeda, S. The evolution of the China Basin and the Mesozoic paleogeography of Borneo. *Earth Planet. Sci. Lett.* **1973**, *18*, 365–376. [CrossRef]
46. Wang, M.M.; Liu, Z.X. The effects of anisotropy of marine magnetic anomalies on the Curie point depth estimates from spectral analysis. *Acta Geophys.* **2018**, *66*, 1019–1030. [CrossRef]
47. Larsen, H.C.; Mohn, G.; Nirrengarten, M.; Sun, Z.; Stock, J.; Jian, Z.; Klaus, A.; Alvarez-Zarikian, C.A.; Boaga, J.; Bowden, S.A.; et al. Rapid transition from continental breakup to igneous oceanic crust in the South China Sea. *Nat. Geosci.* **2018**, *11*, 782–789. [CrossRef]
48. Zhao, Y.; Ding, W.; Yin, S.; Li, J.; Zhang, J.; Ding, H. Asymmetric post-spreading magmatism in the South China Sea: Based on the quantification of the volume and its spatiotemporal distribution of the seamounts. *Int. Geol. Rev.* **2020**, *62*, 955–969. [CrossRef]
49. Franke, D.; Savva, D.; Pubellier, M.; Steuer, S.; Mouly, B.; Auxietre, J.L.; Meresse, F.; Chamot-Rooke, N. The final rifting evolution in the South China Sea. *Mar. Pet. Geol.* **2014**, *58*, 704–720. [CrossRef]
50. Tapponnier, P.; Lacassin, R.; Leloup, P.H.; Schärer, U.; Dalai, Z.; Haiwei, W.; Xiaohan, L.; Shaocheng, J.; Lianshang, Z.; Jiayou, Z. The Ailao Shan/Red River metamorphic belt: Tertiary left-lateral shear between Indochina and South China. *Nature* **1990**, *343*, 431–437. [CrossRef]
51. Morley, C.K. A tectonic model for the Tertiary evolution of strike–slip faults and rift basins in SE Asia. *Tectonophysics* **2002**, *347*, 189–215. [CrossRef]
52. Li, S.; Li, X.; Zhou, J.; Cao, H.; Liu, L.; Liu, Y.; Sun, G.; Suo, Y.; Li, Y.; Yu, S. Passive magmatism on Earth and Earth-like planets. *Geosyst. Geoenviron.* **2022**, *1*, 100008. [CrossRef]
53. He, E.; Zhao, M.; Qiu, X.; Sibuet, J.C.; Wang, J.; Zhang, J. Crustal structure across the post-spreading magmatic ridge of the East Sub-basin in the South China Sea: Tectonic significance. *J. Asian Earth Sci.* **2016**, *121*, 139–152. [CrossRef]
54. Wang, Q.; Zhao, M.; Zhang, J.; Zhang, H.; Sibuet, J.C.; Li, Z.; He, E.; Qiu, X.; Peng, W.; Chen, G. Breakup mechanism of the northern South China Sea: Evidence from the deep crustal structure across the continent-ocean transition. *Gondwana Res.* **2022**. [CrossRef]
55. Gee, J.S.; Kent, D.V. Source of oceanic magnetic anomalies and the geomagnetic polarity timescale. *Treatise Geophys.* **2007**, *5*, 455–507. [CrossRef]
56. Li, C.F.; Shi, X.; Zhou, Z.; Li, J.; Geng, J.; Chen, B. Depths to the magnetic layer bottom in the South China Sea area and their tectonic implications. *Geophys. J. Int.* **2010**, *182*, 1229–1247. [CrossRef]